

# Nuclear and ion spins in semiconductor nanostructures

M. Poggio, R.C. Myers, G.M. Steeves, N.P. Stern, A.C. Gossard, D.D. Awschalom\*

*Center for Spintronics and Quantum Computation, University of California, Santa Barbara, CA 93106, USA*

Available online 9 November 2006

## Abstract

Spin interactions are studied between conduction band electrons in GaAs heterostructures and local moments, specifically the spins of constituent lattice nuclei and of partially filled electronic shells of impurity atoms. Nuclear spin polarizations are addressed through the contact hyperfine interaction resulting in the development of a method for high-field optically detected nuclear magnetic resonance sensitive to  $10^8$  nuclei. This interaction is then used to generate nuclear spin polarization profiles within a single parabolic quantum well; the position of these nanometer-scale sheets of polarized nuclei can be shifted along the growth direction using an externally applied electric field. In order to directly investigate ion spin dynamics, doped GaMnAs quantum wells are fabricated in the regime of very low Mn concentrations. Measurements of coherent electron spin dynamics show an antiferromagnetic exchange between s-like conduction band electrons and electrons localized in the d-shell of the Mn impurities, which varies as a function of well width.

© 2006 Published by Elsevier B.V.

*PACS:* 76.60.Gv; 03.67.-a; 85.35.-p; 75.30.Et; 71.70.Ej; 75.50.Pp; 78.47.+p; 71.70.Gm; 61.72.Vv

*Keywords:* Dynamic nuclear polarization; ODNMR; Dilute magnetic semiconductors; GaMnAs; Quantum well

## 1. Introduction

GaAs, due to its high electron mobility and direct band gap, is a critical component of today's semiconductor technology; its applications range from integrated circuits operating at microwave frequencies to light-emitting and laser diodes. As the possibility of new devices based on spin has emerged in recent years [1], researchers have turned to GaAs due to its favorable electronic properties and rich spin phenomenology. Experiments in GaAs have revealed conduction electron spin coherence on the order of 100 ns [2], over distances in excess of 100  $\mu\text{m}$  [3], and even across heterointerfaces [4,5]. Electric fields have been used in GaAs/AlGaAs parabolic quantum wells (PQWs) to control the electron spin  $g$ -factor [6,7] and in lateral channels to generate and manipulate spins in the absence of magnetic fields [8,9]. Similar experiments have also led to the observation of the spin Hall effect in GaAs and InGaAs epilayers [10,11]. Experiments in highly confined GaAs systems, known as gate-defined quantum dots, have also

demonstrated long electron spin lifetimes and the ability to manipulate the spin states of single electrons [12–14].

Lest we limit ourselves to electronic spin, note that the spin of lattice nuclei is also responsible for a number of intriguing effects in GaAs, which have been studied over the past 50 years [15–18]. Particularly interesting are phenomena attributable to the contact hyperfine interaction, which couples the itinerant spins in the semiconductor bands to those of the nuclei. Through this interaction, optical excitation can result in the hyperpolarization of nuclear moments [15] enabling the detection of nuclear magnetic resonance (NMR) in GaAs with a sensitivity several orders of magnitude larger than conventional methods provide [19–24]. Recent work, aimed at developing techniques for locally manipulating nuclear polarization, have expanded our knowledge of the microscopic processes taking place between electronic and nuclear spins in low-dimensional structures [25–28]. The ability to perform controlled interactions on small numbers of nuclei is critical for schemes suggesting the use of the semiconductor nuclear spins to store information; in such schemes, mobile band electrons naturally act as mediators used both to probe and modify the nuclear states [29]. GaAs

\*Corresponding author. Tel.: +1 805 893 2121; fax: +1 805 893 4170.  
E-mail address: [awsch@physics.ucsb.edu](mailto:awsch@physics.ucsb.edu) (D.D. Awschalom).

structures provide a promising medium for the application of these ideas with their favorable electronic properties and long nuclear spin lifetimes (ranging up to minutes and hours).

In addition to lattice nuclei, another group of localized moments is fundamental to the physics of GaAs: the spin of shell electrons bound to magnetic dopants. The coupling of these moments to band electrons leads to a variety of phenomena, including, perhaps most importantly, carrier-mediated ferromagnetism in III–V dilute magnetic semiconductors (DMS) [30,31]. These interactions enable striking experimental results demonstrating the external electrical control of ferromagnetism in a thin-film semiconducting alloy [32,33]. While the ferromagnetic transition temperatures in these materials are currently below room temperature, progress is being made towards this milestone. A material with controllable room-temperature ferromagnetism, especially an alloy of GaAs with its well-established electronic applications, would put spin-based interactions in semiconductors firmly in the realm of everyday information technology.

In the context of the aforementioned work, we discuss recent experiments focusing specifically on the interactions of band electrons in GaAs heterostructures with both the spin of lattice nuclei and of electrons bound to impurity atoms. Particular attention is paid to the effects of carrier confinement on these interactions. Our study of the contact hyperfine interaction in quantum wells (QWs) leads to the demonstration of a technique for NMR sensitive far beyond conventional methods [34] and subsequent work in PQWs makes further use of the contact hyperfine interaction to pattern nanometer-scale profiles of nuclear polarization [35].

Experiments discussed here on the s–d exchange interaction between conduction band electrons and Mn impurities in GaMnAs QWs suggest that this exchange energy has both a strong dependence on confinement and is antiferromagnetic [36,37]. The latter result may stimulate the rethinking of current theories for sp–d exchange in GaMnAs [38]. Heterostructures of GaAs play a central role throughout the presented work as a means to confine and control band electrons and their spin.

## 2. Nuclear spin in GaAs heterostructures

### 2.1. Optically detected NMR

The contact hyperfine interaction couples the spin of conduction band electrons in a semiconductor to nuclear spins in the crystalline lattice. Among the many consequences of this coupling are the dynamic spin polarization of the lattice nuclei by optically oriented electron spins and the Overhauser shift in the electron spin resonance frequency. Used together, these effects allow for the optical detection of NMR. The detection sensitivity of this technique is several orders of magnitude better than conventional NMR methods allowing for the measurement

of nuclear spin phenomena in certain semiconductor nanostructures containing too few spins for conventional detection.

For instance, the small number of nuclear spins in QWs and quantum dots makes conventional NMR difficult in these semiconductor nanostructures. The enhancement in nuclear spin polarization achieved through optical pumping mentioned in Section 1 can increase the detection sensitivity of typical radio frequency (RF) probes from a minimum of  $10^{17}$  nuclear spins to  $10^{12}$ . As a result, RF detection of optically pumped GaAs multiple QWs has been achieved [19]. Detection of NMR has also been demonstrated through optical measurements of recombination polarization, either by exciting NMR transitions with a conventional coil [20,39], or by purely optical means [21–24]. In the latter case, an optical field is modulated at the nuclear Larmor frequency resulting in an oscillating electron magnetization. This magnetization interacts with nuclear spins through the contact hyperfine coupling and induces NMR transitions in lieu of an external RF field. While ODNMR provides the high sensitivity typical of optical techniques, it has several limitations. For electron  $g$ -factors and spin lifetimes typical of GaAs structures, ODNMR is only possible at low magnetic fields ( $< 1$  T). In addition, the reliance on radiative recombination for detection makes ODNMR disproportionately sensitive to nuclei located near shallow donors and impurities [40].

Another type of ODNMR is possible using the time-resolved Faraday rotation (FR) of transmitted light polarization [41] to probe nuclear spin polarization. In this detection scheme, FR measures the spin precession frequency of electrons in the conduction band. Nuclear spins act on electron spins through the contact hyperfine interaction altering this frequency and allowing for the precise measurement of nuclear polarization. All-optical versions of this method have been demonstrated in bulk GaAs and in GaAs QWs [25,42,43]. These measurements can be made at high-applied magnetic fields and, unlike measurements of time- and polarization-resolved photoluminescence (PL), they are not limited by the charge recombination time.

An extension of this technique utilizing a RF coil for the excitation of NMR transitions [34]. As in all experiments discussed here, a 250-fs 76 MHz Ti:sapphire laser tuned near the exciton absorption energy produces pulses which are split into pump and probe with a full-width at half-maximum (FWHM) of 8 meV and an average power of 2.0 mW and 100  $\mu$ W, respectively. The linearly (circularly) polarized probe (pump) is modulated by an optical chopper at  $f_1 = 940$  Hz ( $f_2 = 3.12$  kHz). Both beams are focused on the sample surface to an overlapping spot 50  $\mu$ m in diameter with the pump beam injecting polarized electron spins along the sample growth direction. The pinning of the of the initial electron spin polarization  $S$  along the growth direction relies on the fact that pump pulses couple predominantly to heavy hole states, which are split off from light hole states in a QW [42,44]. Small

rotations in the linear polarization of the transmitted probe are measured and are proportional to the component of electron spin polarization in the conduction band along the growth direction. Variation of the pump-probe time delay  $\Delta t$  reveals the time evolution of this spin polarization. The Larmor precession frequency  $\nu_L$  and the inhomogeneous transverse spin lifetime  $T_2^*$  can be extracted from such data.

In Fig. 1 we show the response of the FR of transmitted light through a doped 7.5-nm wide (110) GaAs/AlGaAs QW due to the resonant depolarization of nuclear spins using an RF uncoil. The data represent resonances corresponding to the three isotopes present in the QW,  $^{69}\text{Ga}$ ,  $^{71}\text{Ga}$ , and  $^{75}\text{As}$  along with corresponding satellite peaks resulting from a nuclear electric quadrupolar splitting. The sensitivity of the FR-based ODNMR represents one of its main advantages over conventional luminescence-based methods; analysis of the signal-to-noise ratio and of the nuclear polarizations detected, reveals a sensitivity of  $10^8$  nuclear spins. This technique also provides an excellent way to perform ODNMR measurement at high magnetic fields.

The use of an external RF field allows for the future application of well-developed pulsed-NMR techniques for noise reduction while at the same time exploiting the high sensitivity of FR detection [45]. In addition, the conventional magnetic excitation of nuclear transitions circumvents the complex interactions between electrons and

nuclei, which take place in schemes involving optical excitation. Unlike conventional RF magnetic fields, which induce only dipole transitions, modulated optical fields induce both magnetic dipole transitions and electric quadrupole transitions [21,35,42,43].

## 2.2. Generating highly-localized nuclear polarization

The contact hyperfine interaction is local by its very nature: the coupling is non-zero at the locus of each nucleus and vanishes everywhere else. In semiconductor heterostructures, the electron envelope function plays a direct role in determining the spatial extent of the interaction. Under optical orientation, this coupling produces a nuclear polarization profile whose extent is similarly determined [46]. As a result, this interaction affords us the unique ability to pattern nuclear polarization profiles in the image of the envelope functions of polarized conduction band electrons. Depending on the type of heterostructure used, nanometer-scale polarization profiles should be achieved. Profiles containing sufficiently small numbers of nuclear spins combined with the long spin lifetimes of nuclei in the solid-state may have important implications for the future of dense information storage, both classical and quantum. In addition, control over highly localized interactions between conduction electrons and lattice nuclei may provide a means to manipulate such information. Here we review some of the first experiments performed in this vein.

The effect of spin-polarized electrons on nearby lattice nuclear spins can be expressed in terms of an effective magnetic field  $\mathbf{B}_e$ . This field, which is a manifestation of the contact hyperfine interaction, acts to polarize nuclear spins. Dynamic nuclear polarization (DNP), however, depends on the strength of the hyperfine interaction, which goes as

$$H_{\text{hf}} \propto |\Psi(\mathbf{R})|^2 \mathbf{I} \cdot \mathbf{S}, \quad (1)$$

where  $\Psi(\mathbf{R})$  is the electron envelope function and  $\mathbf{R}$  is the position of the relevant nucleus. The nuclear polarization profile, which develops as a result, has a similar spatial extent: it will be confined to the immediate vicinity of the electron probability density. Therefore, we can imagine controlling the position of a confined envelope function of polarized electron spins and thereby polarizing different regions of the crystal. Furthermore, note that since  $\mathbf{B}_e$  goes as  $|\Psi(\mathbf{R})|^2$ , we can vary this effective field at a nuclear site by controlling the position of the electron envelope function. At resonant drive frequencies we may thus expect to induce nuclear spin transitions in the immediate vicinity of the electron probability density. These concepts are illustrated in Fig. 2 and make up the basis for experiments discussed here and in further detail in Ref. [35].

Here, we use gate voltages to electrically position  $\sim 23$ -nm wide distributions of polarized nuclei over a  $\sim 20$ -nm range in a single PQW. Using optically injected spin-polarized carriers, we exploit the contact hyperfine

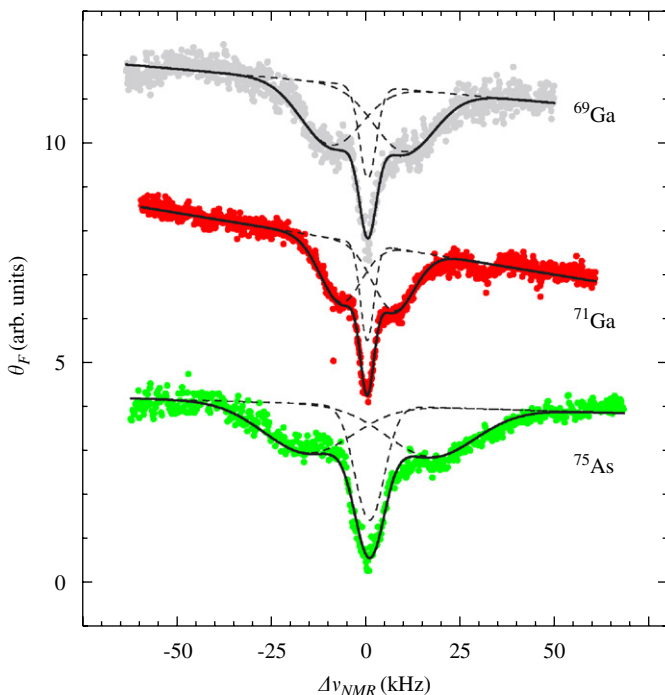


Fig. 1. NMR detected by time-resolved FR in a (110) GaAs/AlGaAs QW. FR plotted as a function of detuning  $\Delta\nu_{\text{NMR}}$  from the  $^{69}\text{Ga}$  resonance of 52.9539 MHz at  $B = 5.2$  T, from the  $^{71}\text{Ga}$  resonance of 67.2898 MHz at  $B = 5.2$  T, and from the  $^{75}\text{As}$  resonance of 54.4992 MHz at  $B = 7.5$  T for the gray, red, and green points, respectively. Solid black lines are fits to the data while dashed lines show the three peaks included in those fits.

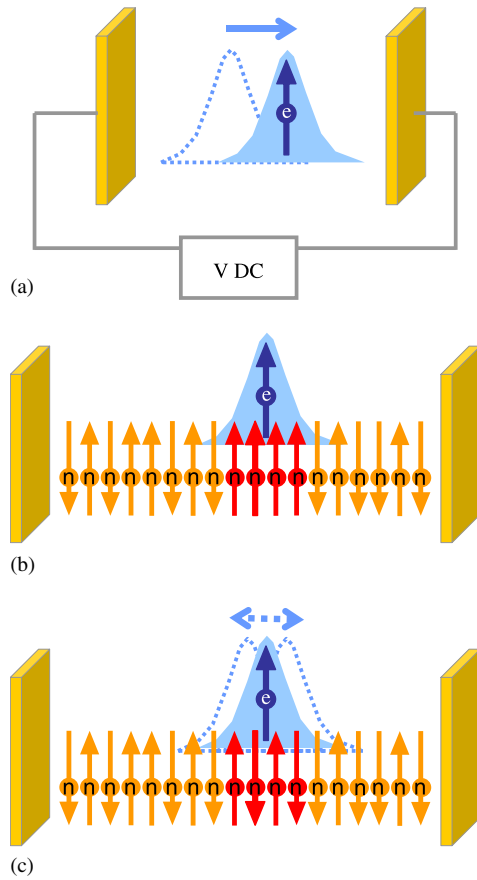


Fig. 2. We imagine a device in which we can control the local interactions between electronic and nuclear spin with an applied voltage by (a) moving the electron envelope function using a pair of external gates, (b) locally polarizing the spin of lattice nuclei, and (c) resonantly inducing nuclear spin transitions.

interaction to produce nuclear polarization in the vicinity of their confined envelope functions [46]. The thin sheets of polarized nuclei are laterally defined by the 50- $\mu\text{m}$  diameter of the focused laser spot. Data showing the measurement of a position-dependent nuclear polarization within a PQW are presented in Fig. 3. The contribution to the electron Larmor precession frequency due to nuclear polarization,  $\nu_n$ , is extracted from time-resolved measurements of FR similar to those described in Section 2.1. The qualitative agreement of the data with theoretical predictions [47] points to our ability to use localized spin-polarized electrons to orient nanometer-scale profiles of nuclear spin. Extending such techniques from systems with one-dimensional confinement (QWs) to systems with higher degrees of confinement (quantum wires and quantum dots) may allow for the controllable polarization of drastically fewer nuclear spins. The application of resonant RF voltages to the gates provides additional electrical control over nuclear spin. In this case, nuclear depolarization is observed upon the application of a resonant RF voltage and is attributed to a local charge-mediated quadrupolar interaction [35].

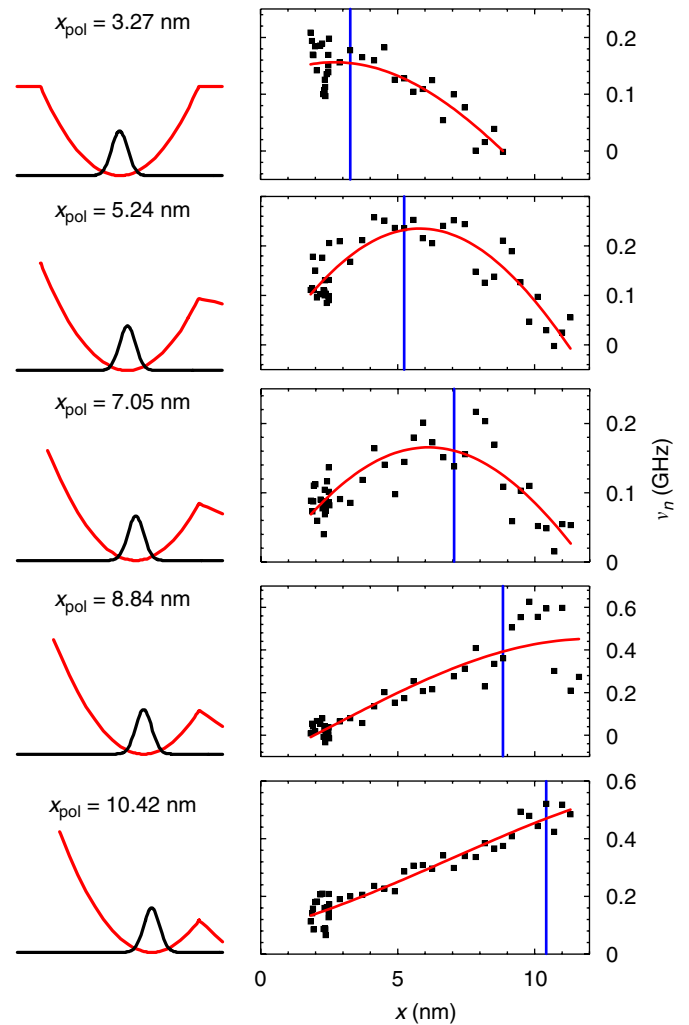


Fig. 3. Measurements of the nuclear polarization distribution within a PQW. In the left column the electron envelope function is shown schematically, centered at different positions  $x_{\text{pol}}$ . Corresponding nuclear polarization distributions are created at  $B = 3.98$  T by polarizing nuclei for 20 min at position  $x_{\text{pol}}$  (blue line). Nuclear polarization is measured as an Overhauser shift  $\nu_n$  and is plotted as a function of  $x$  (solid points). Red curves are Gaussian fits to the data with a fixed FWHM of 23 nm. Centers of the Gaussian fits are 2.7, 5.8, and 6.1, 12.1 and 16.6 nm from top to bottom.

### 3. Mn impurity spin in GaMnAs heterostructures

#### 3.1. Background

The introduction of magnetic dopants into semiconductors allows for the study of interactions between itinerant and localized spins. DMS are semiconducting alloys in which a fraction of the cation sites are occupied by magnetic ions. The spin of electrons localized in the partially filled shells of the substitutional impurities couples to the spin of carriers in both the conduction and valence bands. As a result, electronic Zeeman splittings are enhanced leading to dramatic spin-dependent properties including giant FR, the magnetic-field-induced metal–insulator transition, and the formation of magnetic polarons.

Most importantly, however, the discovery of ferromagnetism in zinc-blende III–V and II–VI Mn-based compounds and the realization that this collective magnetic behavior is mediated by delocalized or weakly localized holes, has given a technological impetus for developing a clear picture of the carrier–shell exchange couplings. In these systems the exchange between the s-like conduction band or p-like valence band and the d shell of the  $\text{Mn}^{2+}$  are known as the s–d and p–d exchange parameters, respectively. In addition to offering an ideal system in which to study the interactions between localized and delocalized spin, DMS offer the prospect of a room-temperature ferromagnetic semiconductor whose ferromagnetic state can be switched on or off by changes in carrier concentration. Such a material would have far-reaching implications on the semiconductor industry and would propel spintronics into the mainstream of computing technology.

In this section we treat the recent development of GaMnAs QWs and the measurement of their s–d and p–d exchange couplings. In II–VI DMS, the s–d and p–d exchange energies are readily measurable and have been characterized in detail through magneto-optical spectroscopy. These materials benefit from high Mn solubility and the electrical neutrality of Mn impurities upon incorporating into the lattice. High concentrations of Mn-doping are achievable, making the effects of s–d and p–d exchange large and easily measurable.

The situation in the III–V alloy GaMnAs is more complex. The presence of Coulomb potentials centered on the magnetic ions as well as on compensating donors introduces an additional obstacle to the interpretation of measurements. More importantly, as a consequence of the low solubility of Mn in GaAs, molecular beam epitaxy (MBE) growth is typically performed at low substrate temperatures ( $\sim 250^\circ\text{C}$ ) and high arsenic overpressures. In this regime of growth defects, such as excess As and Mn interstitials, are incorporated into the epilayers at concentrations that quench sensitive optical signals, including PL and absorption. Therefore characterization of the exchange parameters through optical techniques is problematic in these materials. Despite this constraint, several estimates of the p–d exchange constant have been published from modeling of transport [48], core-level photoemission [49], and cyclotron resonance measurements [50]. A previous study on highly dilute  $\text{Ga}_{1-x}\text{Mn}_x\text{As}$  ( $x < 0.2\%$ ) crystals grown by the Czochralski method reports polarized magnetorelectance data from which the total exciton spin splitting is determined to within 600 meV [51]. This measurement of the collective sp–d energy, however, includes no independent measurements of the s–d and p–d exchange constants ( $N_0\alpha$  and  $N_0\beta$ , respectively); the reported estimation of  $N_0\beta$  depends on an assumed positive value of  $N_0\alpha$  based on work in II–VI DMS.

### 3.2. Mn-doped QWs

In our work, MBE growth conditions are optimized in order to produce GaMnAs in which coherent spin

dynamics can be observed optically, while at the same time incorporating enough Mn to make the effects of s–d and p–d couplings observable. Two types of QW structures are studied, GaMnAs/AlGaAs and InGaMnAs/GaAs. By combining FR measurements of electron spin dynamics with secondary ion mass spectroscopy (SIMS) measurements of these materials both the sign and magnitude of the s–d coupling are determined. The study of QWs of several different widths reveal the dependence of this energy on the carrier confinement.

Using FR spectroscopy to measure the spin-splitting energy of conduction electrons in QWs with various Mn concentrations  $x$  and widths  $w$ ,  $N_0\alpha$  is determined to be negative in both GaMnAs and InGaMnAs QWs. An example of the data is shown in Fig. 4. In addition,  $N_0\alpha$  is seen to grow more negative the narrower the QW, while saturating for wide QWs. In II–VI DMS QWs, a negative change in  $N_0\alpha$  as large as  $-170\text{ meV}$  was previously reported for increasing confinement and was attributed to a kinetic exchange coupling due to the admixture of valence and conduction band wave functions [52].

We plot  $N_0\alpha$  as a function of the electron kinetic energy ( $E_c$ ) for GaMnAs QWs in Fig. 5, and the data are roughly linear. Here,  $E_c$  is defined as the energy between the bottom of the conduction band in the GaAs QW and the ground state energy, which is calculated using a one-dimensional Poisson–Schrödinger solver and the material and structural parameters of the QWs. Extrapolating to  $E_c = 0$  we obtain a bulk value of  $N_0\alpha = -22 \pm 8\text{ meV}$  for GaMnAs. A change in  $N_0\alpha$  as large as  $-185\text{ meV}$ , relative to the extrapolated value for  $E_c = 0$ , is observed in the narrowest wells measured ( $w = 3\text{ nm}$ ). Since  $N_0\alpha > 0$  in bulk II–VI DMS, the kinetic exchange effect appears as a reduction of  $|N_0\alpha|$ , and is expected to cross through zero for very large confinement. Rather than a reduction, we observe an increase in  $|N_0\alpha|$  in GaMnAs QWs. This observation is consistent with the negative contribution of the kinetic exchange predicted by Merkulov et al., since we measure  $N_0\alpha < 0$  in our samples.

### 3.3. An antiferromagnetic s–d coupling?

There is a difference in the behavior of the exchange couplings for the conduction and valence bands in II–VI DMS which is rooted in the nature of exchange interactions between localized spins on impurity sites and the spins of band electrons:

$$H_{\text{ex}} = -\frac{1}{\hbar^2} J \mathbf{S} \cdot \mathbf{M}, \quad (2)$$

where  $J$  is the exchange coupling constant,  $\mathbf{S}$  is the spin of a band electron, and  $\mathbf{M}$  the spin shell electrons on a Mn impurity. Here, we have written the interaction in its simplified two-particle form. Two mechanisms contribute to the value of  $J$ : (1) a normal (direct) exchange mechanism originating from the interaction potential between band and d-shell electrons proportional to the inverse of their

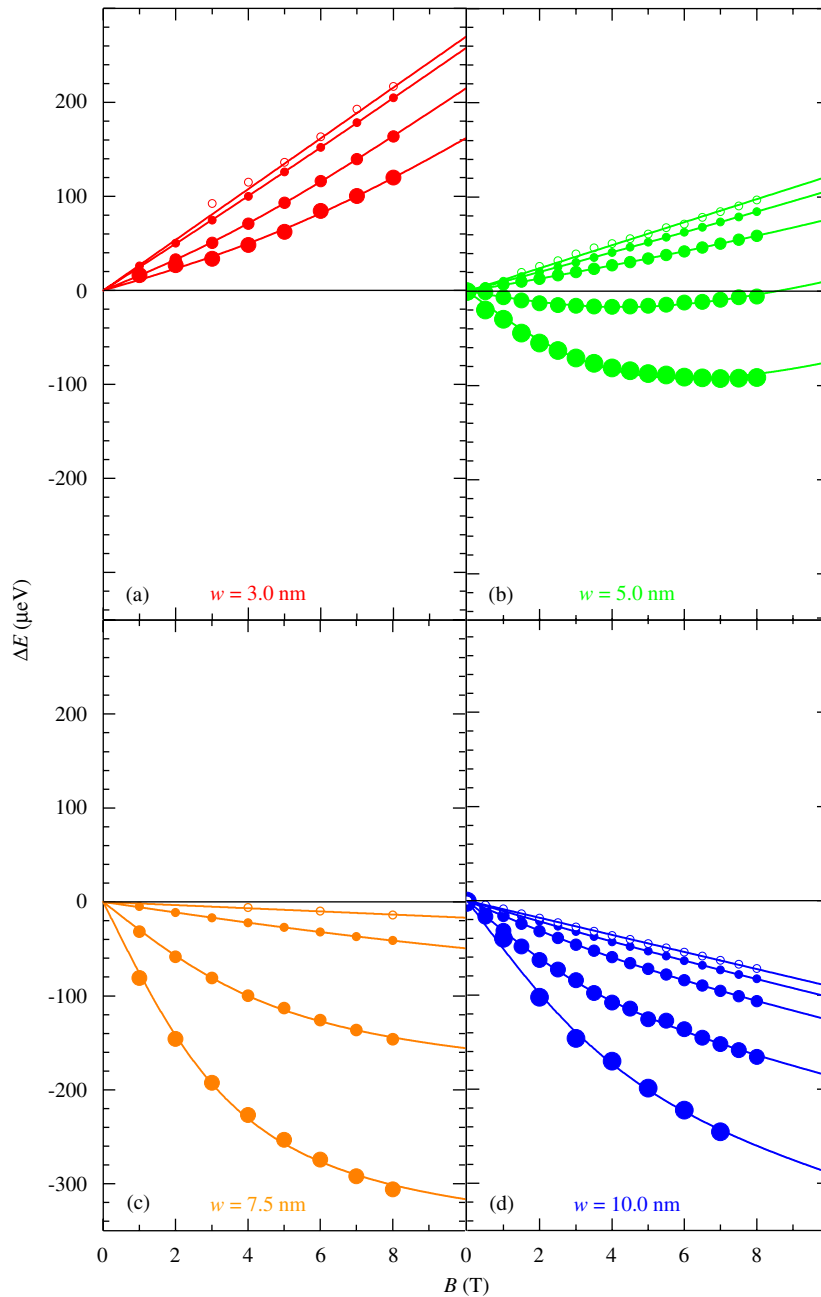


Fig. 4. Spin splitting energy  $\Delta E$  as a function of  $B$  at  $T = 5$  K for GaAs/AlGaAs QWs of different widths with and without Mn doping (solid and open circles, respectively); larger points indicate increasing Mn doping  $x$ . Fits are shown as lines.

separation; and (2) a resonant scattering mechanism due to hybridization between the band and d-shell electrons occurring when the d-level is close to a band edge [53,54]. The first mechanism results in a positive (ferromagnetic) exchange and the second in a negative (antiferromagnetic) exchange. In general both mechanisms contribute to the total exchange  $J$ . In II–VI DMS, the resonant scattering mechanism does not contribute to the conduction band exchange, which is dominated by the normal exchange. Thus a positive exchange is measured in CdMnTe, for example:  $N_0\alpha = 0.22$  eV. In contrast, since the localized d-level falls within the valence band in these systems, the resonant scattering mechanism dominates the exchange for

the valence band resulting in a negative interaction energy:  $N_0\beta = -0.88$  eV. These energies are of the same order for all II–VI compounds containing Mn [55].

The above reasoning makes the extrapolation of our measurements to a bulk GaMnAs exchange of  $N_0\alpha = -23 \pm 8$  meV surprising. The value has a much smaller magnitude and most importantly the opposite sign than values predicted by s–d exchange theories in DMS. Since direct exchange should dominate in the conduction band,  $N_0\alpha$  is expected to be positive. We must therefore consider that some of the assumptions which are valid in II–VI do not apply in GaMnAs. For instance, theoretical efforts are currently underway treating the effects of a

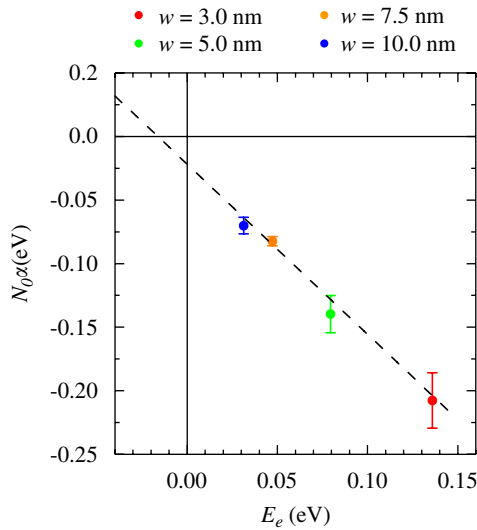


Fig. 5. The effect of confinement on the measured s–d exchange coupling.  $N_0\alpha$  extracted from fits in Fig. 4 and plotted as a function of electron kinetic energy for GaMnAs QWs.

possible hybridization between s-like conduction band states and an excited state of the Mn shell electrons. Such a hybridization could lead to a resonant-scattering contribution in the conduction exchange coupling, explaining the measurement of a negative  $N_0\alpha$ . It is also possible that the smaller band-gap energy in GaMnAs compared to II–VI systems and the correspondingly stronger admixture of valence band states to the conduction band explains the measured negative s–d exchange.

### 3.4. The effects of confinement on s–d exchange

As mentioned in Section 3.2, increasing confinement in II–VI DMS nanostructures results in the reduction in strength of the s–d exchange interaction between conduction electrons and electrons localized in the d-shell of Mn impurities [52]. This reduction is due to an enhancement of the electron kinetic energy by the dimensional quantization of states in a confined system. For conduction band states the dependence of the exchange coupling on carrier kinetic energy results in a decrease in the magnitude of the exchange energy for an increase in the kinetic energy [56]. Though theoretical models of kinetic exchange based on these principles replicate the qualitative features of the data in II–VI materials, their predictions fall short by a factor of  $\sim 5$  [57].

A more complete model also takes into account the effects of the admixture of valence band states to the conduction band states [52]. For states with non-zero  $k$ , the p-like orbitals of the valence band admix to the Bloch functions of the conduction band. Due to the dominance of the resonant scattering mechanism in the valence band, these states contribute a negative energy to the total exchange. As electron kinetic energy (and thus  $k$ ) increases and the admixture of valence band states becomes stronger, so does the negative contribution to the exchange energy.

This negative shift in  $N_0\alpha$  with increasing  $E_c$  contrasts the simple reduction in magnitude predicted for pure conduction band states. Therefore, depending on the degree of the admixture, a positive conduction band exchange constant can decrease and even become negative with increasing kinetic energy. Predictions made by this model agree quantitatively with the experimental data available in II–VI DMS.

Though there are a number of important differences between GaMnAs and the II–VI systems to which the theory of kinetic exchange has been applied, the model by Merkulov et al. which includes the admixture of valence band states into the conduction band fit well to our measurements once the correct material parameters and a single adjustable parameter are used. As evident from Fig. 5,  $N_0\alpha$ , which we measure to be negative in all our experiments, becomes more negative with increasing kinetic energy  $E_c$ , just as predicted by this model. The earlier model of Bhattacharjee et al., which ignores the aforementioned admixture of states, predicts a reduction in  $|N_0\alpha|$  with increasing  $E_c$  and proves to be inconsistent with our findings.

Experimental efforts are currently underway to make more detailed measurements of the dependence of  $N_0\alpha$  on  $E_c$  in GaMnAs and InGaMnAs QWs. We are also making measurements of  $N_0\alpha$  as a function of  $E_c$  in GaMnAs QWs by varying the QW depth instead of the QW width. Such measurements provide further insight on the nature of the dependence and its functional form. Preliminary results show that measurements of  $N_0\alpha$  in GaAs/AlGaAs samples with lower barriers (10% and 20% Al) follow the same dependence shown in Fig. 5. Therefore, regardless of the manner in which we alter the confinement energy, its effect on  $N_0\alpha$  is observed to be the same. While confinement is found to alter the s–d exchange energy in all our experiments, measurements indicate that the interaction remains isotropic regardless of reduced degrees of freedom.

## 4. Conclusion

Here we present experimental data showing our ability to control local interactions between electrons and nuclear spin in a PQW with an externally applied gate voltage. Quasi-static bias voltages allow the patterning of nanometer-size nuclear spin distributions. In addition, we demonstrate the growth of III–V GaMnAs heterostructures in which coherent electron spin dynamics can be observed. The measured s–d exchange coupling is antiferromagnetic in GaMnAs and InGaMnAs QWs. Strong evidence is presented of a direct relation between the conduction band exchange constant and the electron kinetic energy due to one-dimensional quantum confinement.

## References

- [1] D.D. Awschalom, D. Loss, N. Samarth (Eds.), *Semiconductor Spintronics and Quantum Computation*, Springer, Berlin, 2002.

- [2] J.M. Kikkawa, D.D. Awschalom, *Phys. Rev. Lett.* 80 (1998) 4313.
- [3] J.M. Kikkawa, D.D. Awschalom, *Nature* 397 (1999) 139.
- [4] I. Malajovich, J.M. Kikkawa, D.D. Awschalom, J.J. Berry, N. Samarth, *J. Appl. Phys.* 87 (2000) 5073.
- [5] I. Malajovich, J.J. Berry, N. Samarth, D.D. Awschalom, *Nature* 411 (2001) 770.
- [6] G. Salis, Y. Kato, K. Ensslin, D.C. Driscoll, A.C. Gossard, D.D. Awschalom, *Nature* 414 (2001) 619.
- [7] Y. Kato, R.C. Myers, D.C. Driscoll, A.C. Gossard, J. Levy, D.D. Awschalom, *Science* 299 (2003) 1201.
- [8] Y. Kato, R.C. Myers, A.C. Gossard, D.D. Awschalom, *Nature* 427 (2004) 50.
- [9] Y. Kato, R.C. Myers, A.C. Gossard, D.D. Awschalom, *Phys. Rev. Lett.* 93 (2004) 176601.
- [10] Y. Kato, R.C. Myers, A.C. Gossard, D.D. Awschalom, *Science* 306 (2004) 1910.
- [11] J. Wunderlich, B. Kaestner, J. Sinova, T. Jungwirth, *Phys. Rev. Lett.* 94 (2005) 047204.
- [12] T. Fujisawa, D.G. Austing, Y. Tokura, Y. Hirayama, S. Tarucha, *Nature* 419 (2002) 278.
- [13] J.M. Elzerman, R. Hanson, L.H.W. van Beveren, B. Witkamp, L.M.K. Vandersypen, L.P. Kouwenhoven, *Nature* 430 (2004) 431.
- [14] J.R. Petta, A.C. Johnson, J.M. Taylor, E.A. Laird, A. Yacoby, M.D. Lukin, C.M. Marcus, M.P. Hanson, A.C. Gossard, *Science* 309 (2005) 2180.
- [15] G. Lampel, *Phys. Rev. Lett.* 20 (1968) 491.
- [16] E. Brun, R.J. Mahler, H. Mahon, W.L. Pierce, *Phys. Rev.* 129 (1963) 1965.
- [17] M.I. Dyakonov, V.I. Perel, V.I. Berkovits, V.I. Safarov, *Zh. Eksp. Teor. Fiz. Pis'ma* 67 (1974) 1912.
- [18] F. Meier, B.P. Zakharchenya, Elsevier, Amsterdam, 1984.
- [19] S.E. Barrett, R. Tycko, L.N. Pfeiffer, K.W. West, *Phys. Rev. Lett.* 72 (1994) 1368.
- [20] A.I. Ekimov, V.I. Safarov, *Zh. Eksp. Teor. Fiz. Pis'ma* 15 (1972) 257; *JETP, Letters* 15 (1972) 179.
- [21] M. Eickhoff, B. Lenzman, G. Flinn, D. Suter, *Phys. Rev. B* 65 (2002) 125301.
- [22] V.K. Kalevich, V.D. Kul'kov, V.G. Fleisher, *Sov. Phys. Solid State* 22 (1980) 703.
- [23] V.K. Kalevich, V.D. Kul'kov, V.G. Fleisher, *Sov. Phys. Solid State* 23 (1981) 892.
- [24] V.K. Kalevich, *Sov. Phys. Solid State* 28 (1986) 1947.
- [25] J.M. Kikkawa, D.D. Awschalom, *Science* 287 (2000) 473.
- [26] R.K. Kawakami, Y. Kato, M. Hanson, I. Malajovich, J.M. Stephens, E. Johnston-Halperin, G. Salis, A.C. Gossard, D.D. Awschalom, *Science* 294 (2001) 131.
- [27] K.R. Wald, L.P. Kouwenhoven, P.L. McEuen, N.C. van der Vaart, C.T. Foxon, *Phys. Rev. Lett.* 73 (1994) 1011.
- [28] J.H. Smet, R.A. Deutschmann, F. Ertl, W. Wegscheider, G. Abstreiter, K. von Klitzing, *Nature* 415 (2002) 281.
- [29] J.M. Taylor, C.M. Marcus, M.D. Lukin, *Phys. Rev. Lett.* 90 (2003) 206803.
- [30] Y. Ohno, R. Terauchi, T. Adachi, F. Matsukura, H. Ohno, *Phys. Rev. Lett.* 83 (1999) 4196.
- [31] H. Ohno, *Science* 281 (1998) 951.
- [32] H. Ohno, D. Chiba, F. Matsukura, T. Omiya, E. Abe, T. Dietl, Y. Ohno, K. Ohtani, *Nature* 408 (2000) 944.
- [33] D. Chiba, M. Yamanouchi, F. Matsukura, H. Ohno, *Science* 301 (2003) 943.
- [34] M. Poggio, D.D. Awschalom, *Appl. Phys. Lett.* 86 (2005) 182103.
- [35] M. Poggio, G.M. Steeves, R.C. Myers, Y. Kato, A.C. Gossard, D.D. Awschalom, *Phys. Rev. Lett.* 91 (2003) 207602.
- [36] R.C. Myers, M. Poggio, N.P. Stern, A.C. Gossard, D.D. Awschalom, *Phys. Rev. Lett.* 95 (2005) 017204.
- [37] M. Poggio, R.C. Myers, N.P. Stern, A.C. Gossard, D.D. Awschalom, *Phys. Rev. B* 72 (2005) 235313.
- [38] C. Sliwa, T. Dietl, *cond-mat/0505126* (2005).
- [39] D. Paget, G. Lampel, B. Sapoval, V.I. Safarov, *Phys. Rev. B* 15 (1977) 5780.
- [40] D. Paget, *Phys. Rev. B* 25 (1982) 4444.
- [41] S.A. Crooker, D.D. Awschalom, J.J. Baumberg, F. Flack, N. Samarth, *Phys. Rev. B* 56 (1997) 7574.
- [42] G. Salis, D.D. Awschalom, Y. Ohno, H. Ohno, *Phys. Rev. B* 64 (2001) 195304.
- [43] G. Salis, D.T. Fuchs, J.M. Kikkawa, D.D. Awschalom, *Phys. Rev. Lett.* 86 (2001) 2677.
- [44] X. Marie, T. Amand, J. Barrau, P. Renucci, P. Lejeune, *Phys. Rev. B* 61 (2000) 11605.
- [45] H. Sanada, Y. Kondo, S. Matsuzaka, K. Morita, C.Y. Hu, Y. Ohno, H. Ohno, *Phys. Rev. Lett.* 96 (2006) 067602.
- [46] I. Tifrea, M.E. Flatte, *Phys. Rev. Lett.* 90 (2003) 237601.
- [47] I. Tifrea, M.E. Flatte, private communication.
- [48] F. Matsukura, H. Ohno, A. Shen, Y. Sugawara, *Phys. Rev. B* 57 (1998) 2037(R).
- [49] J. Okabayashia, A. Kimura, O. Rader, T. Mizokawa, A. Fujimori, T. Hayashi, M. Tanaka, *Phys. Rev. B* 58 (1998) R4211.
- [50] M.A. Zudov, J. Kono, Y.H. Matsuda, T. Ikaida, N. Miura, H. Munekata, G.D. Sanders, Y. Sun, C.J. Stanton, *Phys. Rev. B* 66 (2002) 161307(R).
- [51] J. Szczytko, W. Mac, A. Stachow, A. Twardowski, P. Becla, J. Tworzydło, *Solid State Commun.* 99 (1996) 927.
- [52] I.A. Merkulov, D.R. Yakovlev, A. Keller, W. Ossau, J. Heurts, A. Waag, G. Landwehr, G. Karczewski, T. Wojtowicz, J. Kossut, *Phys. Rev. B* 83 (1999) 1431.
- [53] B. Coqblin, C.F. Ratto, *Phys. Rev. Lett.* 21 (1968) 1065.
- [54] A.K. Bhattacharjee, G. Fishman, B. Coqblin, *Physica* 117B and 118B (1983) 449.
- [55] J.K. Furdyna, *J. Appl. Phys.* 64 (1988) R29.
- [56] A.K. Bhattacharjee, *Phys. Rev. B* 41 (1990) 5696.
- [57] A.K. Bhattacharjee, *Phys. Rev. B* 58 (1998) 15660.